Hindawi Publishing Corporation
EURASIP Journal on Advances in Signal Processing
Volume 2007, Article ID 12145, 15 pages
doi:10.1155/2007/12145

Research Article

Fast Burst Synchronization for Power Line Communication Systems

Gerd Bumiller[1] and Lutz Lampe[2]

[1] *iAd GmbH, 90613 Großhabersdorf, Germany*
[2] *Department of Electrical and Computer Engineering, University of British Columbia, Vancouver, Canada V6T 1Z4*

Received 1 November 2006; Accepted 28 February 2007

Recommended by Halid Hrasnica

Fast burst synchronization is an important requirement in asynchronous communication networks, where devices transmit short data packets in an unscheduled fashion. Such a synchronization is typically achieved by means of a preamble sent in front of the data packet. In this paper, we study fast burst synchronization for power line communication (PLC) systems operating below 500 kHz and transmitting data rates of up to about 500 kbps as it is typical in various PLC network applications. In particular, we are concerned with the receiver processing of the preamble signal and the actual design of preambles suitable for fast burst synchronization in such PLC systems. Our approach is comprehensive in that it takes into account the most distinctive characteristics of the power line channel, which are multipath propagation, highly varying path loss, and disturbance by impulse noise, as well as important practical constraints, especially the need for spectral shaping of the preamble signal and fast adjustment of the automatic gain control (AGC). In fact, we regard the explicit incorporation of these various requirements into the preamble design as the main contribution of this work. We devise an optimization criterion and a stochastic algorithm to search for suitable preamble sequences. A comprehensive performance comparison of a designed and two conventional preambles shows that the designed sequence is superior in terms of (a) fast burst synchronization in various transmission environments, (b) fast AGC adjustment, and (c) compliance of its spectrum with the spectral mask applied to the data transmit signal.

1. INTRODUCTION

In many distributed communication systems relatively short bursts or packets of data are transmitted asynchronously and packet acquisition, or *burst synchronization*, has to be performed for each individual packet. A "fast" and reliable synchronization method is therefore mandatory to avoid undue signaling overhead and excessive packet loss. Typically, a well-designed preamble signal, which precedes the data block, is employed for this purpose. While preamble sequences with good autocorrelation properties are often considered for burst synchronization in frequency-nonselective channels (e.g., [1, 2]), repetition preambles are commonly employed for frequency-selective channels (e.g., [3–6]). The latter are often used in combination with orthogonal frequency division multiplexing (OFDM) and also support other synchronization tasks like carrier frequency synchronization (cf., e.g., [7] and references therein).

In this paper, we consider fast burst synchronization for OFDM-based power line communication (PLC) systems. We assume that the PLC network consists of many devices which communicate in an unscheduled fashion, which is the reason for aiming at *fast* synchronization, and with relatively low data rates (say below 500 kbps). This includes, for example, automatic meter reading (AMR), real-time energy management, home automation, and also potential automotive PLC systems (cf., e.g., [8–11]). The power line channel is typically characterized by multipath propagation due to signal reflections at impedance mismatches and distance and frequency dependent path loss (cf., e.g., [12]). Severe frequency selectivity is also caused by simultaneous transmissions in single-frequency networks (SFNs) [13], whose application is envisaged for PLC systems extending over a relatively large area [14], as it is often the case in AMR and energy-management systems mentioned above. Furthermore, short-term and long-term time channel variations (e.g., [15, 16]) and various

kinds of impulse noise are observed in PLC systems (e.g., [17]).

These characteristics of the power line channel make fast burst synchronization a challenging task. Multipath propagation spreads the channel energy over several (baseband) modulation intervals, which makes the problem of finding a correlation peak more difficult. This is particularly true since, due to variations over time, the channel impulse response is unknown at the receiver. While repetition preambles, that is, periodic preambles, alleviate this problem, they are relatively long, for example, 160 samples in IEEE 802.11a [4] and 192 samples in IEEE 802.15.3 [5], causing considerable overhead when short packets are sent. The large variations in path loss experienced at different locations in a PLC network and high amplitude peaks of impulse noise necessitate automatic gain control (AGC) with a large dynamic range at the receiver. Hence, the problem of fast burst synchronization is compounded by the need for fast AGC adjustment.

Deeming repetition preambles as too inefficient, in this paper we consider the design of preambles with peak-like correlation properties for fast burst synchronization in PLC systems. In this context, we make the following contributions.

(i) We present a design approach that explicitly takes into account the presence of (a) multipath propagation and (b) impulse noise and the need for (c) fast AGC adjustment and also (d) spectral shaping of the preamble signal due to the constraints of practical filtering.

(ii) It follows almost naturally that this comprehensive approach does not lend itself to a rigorous analysis and derivation of a corresponding mathematical optimization problem. Instead, we propose a figure of merit which balances the different demands imposed on the preamble sequence. For optimization with respect to this figure we devise a suboptimal stochastic search algorithm.

(iii) Furthermore, we specify an AGC unit and present a novel synchronization metric, which are particularly adapted to the power line channel characteristics outlined above. This enables us to evaluate the performance of preamble sequences obtained from the optimization and to select the overall best sequence.

(iv) We present a comprehensive performance comparison of one designed example preamble with two commonly used preambles based on a polyphase Barker [18, 19] and a constant amplitude zero autocorrelation (CAZAC) [20] sequence, respectively. This comparison shows that the designed preamble outperforms the conventional preambles in terms of successful detection of a synchronization event, robustness to multipath transmission and false synchronization, and fast AGC adjustment.

Organization

The remainder of this paper is organized as follows. In Section 2, we introduce the basic parameters of the considered OFDM transmission system, and we present the AGC structure and the metric for burst synchronization. The advocated preamble design approach is developed in Section 3. In Section 4, numerical performance results and the comparison with two conventional preambles are presented. Finally, conclusions are given in Section 5.

Notation

The following notation is used in this paper. Bold lower case $\mathbf{x}$ and upper case $\mathbf{X}$ denote vectors and matrices, respectively. $(\cdot)^T$, $(\cdot)^*$, and $(\cdot)^H$ denote transposition, complex conjugation, and Hermitian transposition, respectively. $\det(\mathbf{X})$ is the determinant of a matrix $\mathbf{X}$, $\mathbb{R}\{x\}$ and $\Im\{x\}$ are the real and imaginary parts of a complex number x, respectively, and $\Pr\{\cdot\}$ denotes the probability of the event in brackets. Finally, $\delta[\kappa]$ denotes the Kronecker delta, that is, $\delta[\kappa] = 1$ for $\kappa = 0$ and zero otherwise.

2. TRANSMISSION SYSTEM AND BURST SYNCHRONIZATION

In this section, we first introduce the basic parameters of the considered OFDM system. Then, we describe in detail the AGC unit and the burst synchronization metric that will be used for the design and performance evaluation of preamble signals.

2.1. OFDM transmission system

We consider an OFDM transmission system for low-to-medium data-rate applications like those mentioned in Section 1. More specifically, data rates of about 10 to 500 kbps are assumed, and the occupied frequency band ranges from 9 to 490 kHz, which includes the European CENELEC EN 50065 Bands A to D and bands available in Japan and the USA [21–23]. Concentrating on these frequency bands and data-rate ranges entails that synchronization of carrier and sampling frequency is not critical. Standard local oscillators with frequency offsets of not more than, say, 10 ppm guarantee a sufficiently high signal-to-noise ratio (SNR) without additional synchronization.

While the following discussion and in particular the design and performance evaluation of preambles for fast burst synchronization are applicable to practically any PLC system having these parameters, we mention iAd's OFDM-based system, which is described in some detail in [24], as a specific example that allows communication with configurable data rates and bandwidths in the specified ranges. The number of subcarriers is adjusted flexibly and, as common practice in OFDM transmission systems, the subcarriers at the spectral edges, so-called guard subcarriers, are not used for data transmission. While this relaxes the requirements on subsequent filtering to meet the desired spectral mask, it also has implications on the preamble design (see Section 3.2).

The considered OFDM receiver structure is illustrated in Figure 1. As usual, the received signal $r'(t)$ is first filtered to reject out-of-band noise and other potential adjacent channel interference, and the filter output $r(t)$ is processed for

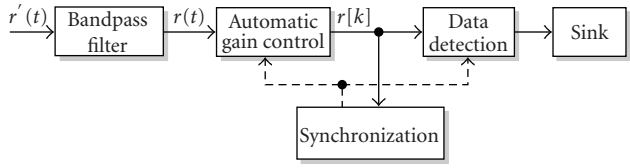

Figure 1: Block diagram of the receiver structure. Dashed lines indicate control signals.

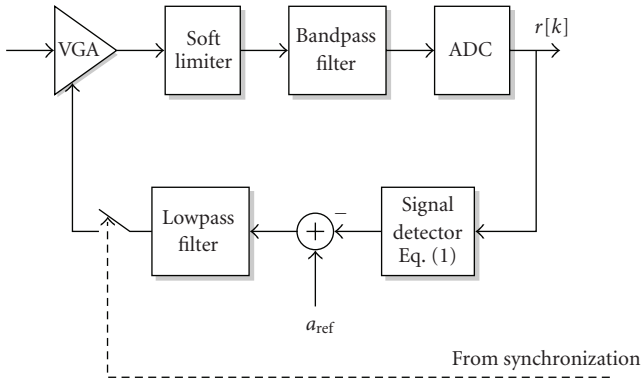

Figure 2: Block diagram of the AGC unit. The dashed line indicates a control signal.

data detection. The components that are involved in the acquisition of an OFDM packet are the AGC and the burst synchronization unit. They are discussed in detail in the following two sections.

2.2. Automatic gain control (AGC)

Due to the wide dynamic range of the received signal, which is often in the order of 120 dB because of line impedance variations and impulse noise, an AGC is a necessity for transmission over power lines.

The block diagram of the AGC is shown in Figure 2, with the classical structure of a variable gain amplifier (VGA), a signal detector, and a loop filter (cf., e.g., [25]). The voltage limitation of the amplifier is taken into account by a subsequent soft limiter. We note that such a limitation, which causes clipping of large peaks of the received signal $r(t)$, is desirable in power line channels as it limits the impact of impulse noise. Furthermore, the amplified and limited signal is filtered to avoid aliasing after subsequent analog-to-digital (AD) conversion due to saturation of the amplifier, that is, due to spectral regrowth of the soft limited signal. The AD converter (ADC) operates on a fixed sampling frequency, which, depending on the carrier frequency f_c and signal bandwidth B_s, is a multiple of the baseband sampling frequency f_s (see Figure 3 and Section 2.3 for down-conversion and sampling). The detector yields an estimate

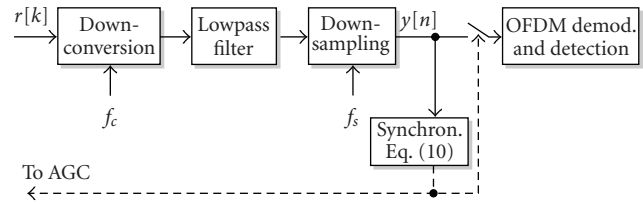

Figure 3: Block diagram of digital down-conversion and further data processing. Dashed lines indicate control signals.

of the short-term average of the amplitude of the digital received signal $r[k]$:

$$\overline{a}[k] = \frac{1}{N_{\mathrm{AGC}}} \sum_{i=0}^{N_{\mathrm{AGC}}-1} |\, r[k-i] \,|. \tag{1}$$

This moving-average filter, which is linear in the input $|r[k]|$, is chosen in order to (a) render the steering variable of the VGA proportional to the amplifier gain, and (b) counter the detrimental effect of impulse noise. In particular, a conventional peak (maximum-hold) detector would adjust the AGC gain too low in the event of an impulsive disturbance. The length N_{AGC} of the filter impulse response influences the loop bandwidth and it is adjusted as function of the required AGC speed measured in baseband-sample intervals. This means that N_{AGC} depends on the preamble structure and on f_s (and thus the signal bandwidth B_s).

The linear average $\overline{a}[k]$ is compared to the reference value a_{ref}. a_{ref} should be chosen such that the full dynamic range of the preamble signal is preserved, while large received signal amplitudes due to impulse noise are suppressed. Hence, it is adjusted such that the preamble signal is just not clipped at the soft limiter. The difference signal $a_{\mathrm{ref}} - \overline{a}[k]$ is an input to a lowpass filter, which is implemented as a PI-circuit with transfer function

$$H(s) = \frac{G_1 s + G_2}{s}. \tag{2}$$

We note that the P-circuit (factor G_1) is necessary for a fast response of the AGC with the moving-average filter in the feedback loop. The parameters G_1 and G_2 of $H(s)$ allow to configure the speed of the AGC depending on the preamble design and the signal bandwidth. In particular, these parameters together with N_{AGC} are adjusted such that the dynamic of the AGC loop measured in baseband-sample intervals is approximately fix, that is, it is approximately independent of the signal bandwidth B_s. This is an important requirement to enable reliable burst synchronization, which is performed using the baseband signal $y[n]$ (see Figure 3 and Section 2.3), to accommodate OFDM signals with highly flexible bandwidths B_s.

Finally, there is a feedback control signal from the synchronization unit to the AGC unit. This basically freezes the VGA gain if the start of an OFDM packet has been detected, that is, it switches the AGC into a linear operation mode.

2.3. Burst synchronization

Let us define the synchronization sequence consisting of N baseband samples as

$$\mathbf{s} \triangleq [s_1\, s_2\, \cdots s_N]^T. \tag{3}$$

While the design of the synchronization sequence is discussed in detail in Section 3, two desirable properties of $\mathbf{s}$ should already be mentioned at this point. First, the synchronization sequence should provide for a correlation gain. Defining the aperiodic autocorrelation function as

$$\varphi[\kappa] \triangleq \sum_{i=1}^{N-\kappa} s_i s_{i+\kappa}^*, \quad 0 \le \kappa \le N-1, \tag{4}$$

this means that the peak side lobe $\max_{\kappa>0}\{|\varphi[\kappa]|\}$ should be small (cf., e.g., [2, 26] for related merit factors). Second, the peak amplitude of the synchronization sequence should be limited. More specifically, we require that

$$|s_i| \approx \text{constant}, \quad 1 \le i \le N. \tag{5}$$

We note, however, that a strictly constant-amplitude synchronization sequence is not feasible due to the spectral forming requirements (see Section 3.2).

The input to the synchronization unit is the equivalent complex baseband signal $y[n]$, which is obtained after digital down-conversion of $r[k]$ from carrier frequency f_c to the baseband and down-sampling with sampling frequency f_s as it is shown in Figure 3. For the detection of an OFDM data packet the magnitude of the correlation of $y[n]$ with the synchronization sequence $\mathbf{s}$, that is,

$$M[n] = \left| \sum_{i=0}^{N-1} y[n-i] s_{N-i}^* \right| \tag{6}$$

could be formed and compared with a threshold (e.g., [2]). However, considering the large dynamic range of $y[n]$ even after the AGC, the comparison with an absolute threshold is not advisable. Instead, an energy normalized metric (recall that $|s_i|$ is approximately constant)

$$M_{\text{norm}}[n] = \frac{M[n]}{\sqrt{\sum_{i=0}^{N-1} |y[n-i]|^2}} \tag{7}$$

is preferable to prevent locking onto noise, especially in the case of an impulse noise event. We note that an energy normalization of individual samples $y[n]$ is not practicable, even if the synchronization sequence was a constant amplitude signal, since multipath transmission results in a nonconstant amplitude of the desired part of the received signal.

However, in multipath channels, due to multiple signal *reflections* along the power line [12] or because of multiple simultaneous signal *transmissions* in an SFN [14], the metric $M_{\text{norm}}[n]$ in (7) is not a viable solution. This can be seen from considering the idealized scenario of (a) an overall linear channel (neglecting nonlinear effects due to AGC) without additive noise so that

$$y[n] = \sum_{l=0}^{L'-1} h[l] s_{n-n_0-l+1}, \tag{8}$$

where $h[l]$ is the channel impulse response and n_0 denotes the packet arrival time, and (b) asymptotically long synchronization sequences ($N \to \infty$) with $\varphi[\kappa] \to \delta[\kappa]$, for which we obtain

$$M_{\text{norm}}[n] = \frac{|h[n-n_0-N+1]|}{\sqrt{\sum_{l=0}^{L'-1} |h[l]|^2}}. \tag{9}$$

Clearly, the channel energy $\sum_{l=0}^{L'-1} |h[l]|^2$ is spread over several samples of $M_{\text{norm}}[n]$, which results in a degraded synchronization performance.

To overcome this limitation, another modification of the synchronization metric is necessary. More specifically, we propose to extend the correlation window from N to $N+L-1$ samples and to sum the squared magnitudes of the correlations of $[y[n-l]\ \cdots\ y[n-l-N+1]]$ with $\mathbf{s}$, $0 \le l \le L-1$, to capture the energy of the multipath channel more completely. The appropriately normalized synchronization metric reads

$$\begin{aligned} M_{\text{sync}}[n] &= \frac{\sqrt{\sum_{l=0}^{L-1} |M[n-l]|^2}}{\sqrt{\sum_{i=0}^{N+L-2} |y[n-i]|^2}} \\ &= \frac{\sqrt{\sum_{l=0}^{L-1} \left| \sum_{i=0}^{N-1} y[n-l-i] s_{N-i}^* \right|^2}}{\sqrt{\sum_{i=0}^{N+L-2} |y[n-i]|^2}}. \end{aligned} \tag{10}$$

Of course, neither the channel impulse response $h[l]$ nor its length L' can be assumed known for synchronization. Hence, L is an estimate of L' based on delay spreads measured in typical power line channels. Depending on the bandwidth B_s of the transmit signal, L is chosen between $L_{\min} = 2$ and $L_{\max} = 8$. It is interesting to note that a similar metric, without energy normalization, has been proposed in [27] for timing synchronization for wireless personal area network (WPAN) devices.

The synchronization metric $M_{\text{sync}}[n]$ in (10) will be considered in the following. In particular, if this metric exceeds a certain threshold for the first time, that is,

$$M_{\text{sync}}[n] > t_{\text{sync}}, \tag{11}$$

an OFDM packet is detected and $\widetilde{n}_0 = n - N + 1$ is considered as packet arrival time. In case of such a synchronization event, the AGC will be fixed and the subsequently received signal samples $y[n]$ are passed to the OFDM data detection unit (see control signals in Figures 1–3).

3. PREAMBLE DESIGN

We now turn to the design of the preamble sequence, of which the synchronization sequence $\mathbf{s}$ in (3) is a main part. The basic structure of the preamble is described in Section 3.1 and the constraints that need to be considered for the design are summarized in Section 3.2. The actual design approach and algorithm are presented in Section 3.3.

3.1. Basic structure of the preamble

It appears reasonable to construct the preamble as a concatenation of two parts: a prefix for coarse AGC adjustment

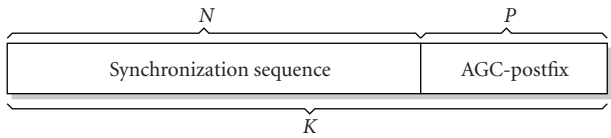

Figure 4: Structure of the considered preamble sequences of $K = N+P$ samples. The synchronization sequence consists of N samples, the AGC-postfix has P samples.

followed by the synchronization sequence $\mathbf{s}$ for start-of-packet detection. If, however, the AGC is adjusted such that the VGA is operated relatively close to its amplitude limits, that is, a_{ref} is relatively large, in order to effectively suppress impulse noise, and assuming a preamble with low peak-to-average power ratio (PAPR), we find that the additional correlation gain from including the prefix into the synchronization sequence outweighs the loss due to the nonlinear effects caused by the AGC during the reception of first samples of the preamble. Accordingly, we omit an extra prefix used for AGC adjustment only.

Instead, we propose to extend the preamble by an AGC-postfix consisting of P baseband samples appended to the synchronization part $\mathbf{s}$. The AGC-postfix is intended for fine adjustment of the AGC very shortly before the AGC gain is fixed for detection of the OFDM packet. In particular, we choose P such that it corresponds to the signal delay due to down-conversion and down-sampling after the AGC. Thus, it is no additional signaling overhead, but it rather allows for an optimal use of the signal processing delay inherent to the receiver.

The resulting preamble structure is shown in Figure 4. We denote the preamble sequence by

$$\mathbf{p} \triangleq [p_1\, p_2\, \cdots\, p_K]^T, \tag{12}$$

where $K = P + N$ is the preamble length and $p_i = s_i$ for $1 \le i \le N$.

3.2. Design constraints and requirements

The preamble design has to take various constraints and requirements into account, which can roughly be classified into constraints and requirements originating from the transmitter, the power line channel, and the receiver.

(1) Transmitter

The preamble should be as short as possible to reduce the signaling overhead and its spectrum should match that of the payload OFDM signal. For example, according to the European CENELEC standard [21], the bandwidth of an OFDM signal is determined by the frequencies at which the magnitudes of the signal spectrum are 20 dB below its maximal value. To meet this spectral mask for a given bandwidth, guard subcarriers at the spectral edges of the OFDM signal are typically used as already mentioned in Section 2.1. Hence, the spectrum of the preamble should only contain very little energy in these guard bands. Furthermore, the PAPR of the preamble signal should be sufficiently small to avoid clipping due to nonlinearities of the transmit amplifier and to transmit the preamble with maximal possible power.

(2) Channel

The preamble needs to be robust to multipath transmission and multiple-transmitter communication in SFNs, which "smears" the correlation peak of the synchronization metric.

(3) Receiver

The preamble should be suitable for fast AGC adjustment, which calls for preferably small variations of the preamble amplitudes. The autocorrelation function of the synchronization sequence should have low side lobes and the correlation peak should not be overly degenerated due to nonlinear distortions caused by the AGC. We also require that the correlation peak should be robust to small frequency offsets between the local oscillators at the transmitter and receiver, since explicit carrier frequency synchronization is not performed as mentioned in Section 2.1. Furthermore, low correlation values for relatively large frequency offsets are desirable to prevent synchronization to adjacent channel signals in PLC networks.

3.3. Design approach

According to the discussion above, a comprehensive design approach has to include the correlation properties of the synchronization part $\mathbf{s}$, the use of the synchronization metric $M_{\text{sync}}[n]$ defined in (10), and the time- and frequency-domain properties of the entire preamble $\mathbf{p}$. Considering that there is no analytical method to construct sequences even if only low aperiodic autocorrelation properties are desired, it is clear from the outset that (a) only a suboptimal optimization can be formulated and (b) a fast computer search needs to be implemented to perform the optimization (cf., e.g., [19, 26, 28] for computer searches for sequences with good autocorrelation properties). Due to the "hard" constraint on the spectral properties of the transmit signal, we choose a frequency-domain design (Section 3.3.1), whose parameters are optimized with a greedy algorithm (Section 3.3.2). Finally, the AGC reference value a_{ref} and the synchronization threshold t_{sync} are determined for an optimized sequence $\mathbf{p}$ (Section 3.3.3).

3.3.1. Frequency-domain design

To comply with the requirement that the spectrum of the preamble signal has to satisfy the spectral mask for the OFDM payload, we design the preamble in the frequency domain. Frequency components at the edges of the frequency band are required to be zero in order to create a guard band, while frequency components within the band are assigned equal power to achieve a quasiconstant power spectral den-

sity. Hence, denoting the ratio of active subcarriers to all subcarriers by d, we require that $d \cdot K$ of the K elements

$$P_\nu \triangleq \sum_{i=1}^{K} p_i e^{-j(2\pi/K)(i-1)(\nu-1)}, \quad 1 \le \nu \le K, \tag{13}$$

of the discrete Fourier transform (DFT) of $\mathbf{p}$ have constant modulus, while the others are zero. More specifically,

$$P_\nu = \begin{cases} e^{j\phi_\nu}, & \text{for } \dfrac{(1-d)}{2}K < \nu \le \dfrac{(1+d)}{2}K, \\ 0, & \text{otherwise,} \end{cases} \tag{14}$$

which results in the preamble sequence

$$p_i = \frac{1}{K} \sum_{\nu=(1-d)K/2+1}^{(1+d)K/2} e^{j\phi_\nu} e^{j(2\pi/K)(i-1)(\nu-1)}. \tag{15}$$

For the numerical evaluations in Section 4 we will adopt $d = 0.82$ as an exemplary and practically relevant value.[1]

We would like to mention that a similar approach was considered in [29, 30] for the design of an OFDM synchronization sequence. Different from (15), the synchronization sequence in [29, 30] is embedded in the OFDM data signal, and hence only a subset of active subcarriers (so-called pilot subcarriers) are available for synchronization. The optimizations were carried out with respect to the positions ν of the pilot subcarriers assuming $\phi_\nu = 0$.

3.3.2. Optimization

The further optimization of $\mathbf{p}$ with elements from (15) is based on a figure of merit, which incorporates the requirements on the preamble sequence listed in Section 3.2, and a simple greedy algorithm is employed to search for preambles with large merit.

(a) Figure of merit

Every trial preamble vector $\mathbf{p}$ is passed through the entire transmitter and receiver chain to generate the corresponding baseband received signal $y[n]$. The effects of digital modulation and filtering, digital-to-analog (DA) and AD conversion and possible clipping are considered by setting the peak value of the transmitted preamble signal $p(t)$ equal to the maximum amplitude of the DA converter (DAC) output. To assess the autocorrelation properties of the synchronization-sequence part of the preamble, the peak-to-side-peak ratios

$$R_{\text{psp}}(L) \triangleq \frac{c_{\text{peak}}(L)}{c_{\text{side-peak}}(L)} \tag{16}$$

with

$$c_{\text{peak}}(L) = \max_{\substack{n\in[n_0+N-1,\\ n_0+N+L-2]}} \left\{ \sum_{l=0}^{L-1} \left| \sum_{i=0}^{N-1} y[n-l-i] s_{N-i}^{*} \right| \right\}, \tag{17}$$

$$c_{\text{side-peak}}(L) = \max_{n<n_0+N-1} \left\{ \sum_{l=0}^{L-1} \left| \sum_{i=0}^{N-1} y[n-l-i] s_{N-i}^{*} \right| \right\} \tag{18}$$

are determined for $L_{\min} \le L \le L_{\max}$. Values $n > n_0+N+L-2$ are not considered for side peaks in (18) since a synchronization will always lock on to the first correlation peak. To account for the dynamic of the transmitted preamble signal $p(t)$ corresponding to the preamble $\mathbf{p}$, which is critical for the transmitter and receiver VGA and the AGC adjustment at the receiver, we consider

$$\begin{aligned} D_1 &\triangleq \int_0^{T_K} |\,p(t)\,|\,dt, \\ D_2 &\triangleq 5 \int_{T_N}^{T_K} |\,\dot{p}(t)\,|\,dt + \int_0^{T_N} |\,\dot{p}(t)\,|\,dt, \\ D_3 &\triangleq 3 \min_{t\in(T_N,T_K)} \{\,|\,p(t)\,|\,\} + \min_{t\in(0,T_N)} \{\,|\,p(t)\,|\,\}, \end{aligned} \tag{19}$$

where T_K and T_N denote the duration of the whole preamble and the synchronization part, respectively, and $\dot{p}(t)$ is the first-order derivative of $p(t)$. Since the maximum amplitude of $p(t)$ is fixed, D_1 and D_2 are measures for the amplitude fluctuations within $p(t)$. While D_1 reflects the absolute variation of the amplitudes, D_2 is an indicator for the rate of amplitude changes. Finally, the occurrence of very small amplitude signals, which is important for AGC adjustment, is considered in D_3. Since quick amplitude changes and small minimum amplitudes can have a detrimental effect for the AGC adjustment particularly during the AGC-postfix, the corresponding terms are weighted with larger factors in D_2 and D_3.

Finally, $R_{\text{psp}}(L)$, D_1, D_2, and D_3 are combined as

$$F = \sum_{L=L_{\min}}^{L_{\max}} R_{\text{psp}}(L) + D_1 + K \cdot D_3 - D_2 \tag{20}$$

and F is considered as the figure of merit according to which preamble sequences are optimized.

We remark that while the requirement for robustness against frequency offset and false synchronization listed in Section 3.2 is not explicitly accounted for in F, we found that frequency-domain design with randomly chosen initial phases (see (b) below) yields fairly robust preamble designs in this regard (see numerical results in Section 4.2).

(b) Greedy algorithm

The greedy optimization algorithm starts with a randomly chosen initial DFT-vector and rotates the DFT-components P_ν successively by $e^{\pm j\Delta\phi}$ and a rotation is retained if the figure

[1] This particular choice is inspired by the parameters in iAd's PLC system [24], where 82% of the OFDM subcarriers are active.

Input: $[K, d, I, \Delta\phi_0, c]$
Output: $\mathbf{p}, F$

Randomly generate phase values ϕ_v, $(1-d)K/2 < v \leq (1+d)K/2$
Current figure of merit: $\hat{F} = 0$, $\widetilde{F} = 0$
// loop for different phase increments
for $m = 1$ to I
  $\Delta\phi_m = \Delta\phi_{m-1}/c$ // update phase increment
  // inner loop with phase increment $\Delta\phi_m$
  do
    $F = \hat{F}$ // update figure of merit
    // loop over all active subcarriers
    for $v = (1-d)K/2 + 1$ to $(1+d)K/2$
      do // rotate by $(+\Delta\phi_m)$
        $\hat{F} = \widetilde{F}$
        $\widetilde{\phi}_v = \phi_v$
        $\phi_v = \widetilde{\phi}_v + \Delta\phi_m$ // trial phase
        // generate trial preamble, (15), and calculate corresponding $\widetilde{F}$, (20)
        $\mathbf{p}$ = generate-preamble($[\phi_{(1-d)K/2+1}, \ldots, \phi_{(1+d)K/2}]$)
        $\widetilde{F}$ = calculate-figure-of-merit($\mathbf{p}$)
      while $(\hat{F} < \widetilde{F})$
      $\widetilde{F} = \hat{F}$ // reset value to last successful trial
      $\phi_v = \widetilde{\phi}_v$ // reset value to last successful trial
      do // rotate by $(-\Delta\phi_m)$
        $\hat{F} = \widetilde{F}$
        $\widetilde{\phi}_v = \phi_v$
        $\phi_v = \widetilde{\phi}_v - \Delta\phi_m$ // trial phase
        // generate trial preamble, (15), and calculate corresponding $\widetilde{F}$, (20)
        $\mathbf{p}$ = generate-preamble($[\phi_{(1-d)K/2+1}, \ldots, \phi_{(1+d)K/2}]$)
        $\widetilde{F}$ = calculate-figure-of-merit($\mathbf{p}$)
      while $(\hat{F} < \widetilde{F})$
      $\widetilde{F} = \hat{F}$ // reset value to last successful trial
      $\phi_v = \widetilde{\phi}_v$ // reset value to last successful trial
    end for
  while $(F < \hat{F})$ // as long as an improvement is achieved
end for
// generate optimized preamble, (15), and calculate corresponding F, (20)
$\mathbf{p}$ = generate-preamble($[\phi_{(1-d)K/2+1}, \ldots, \phi_{(1+d)K/2}]$)
F = calculate-figure-of-merit($\mathbf{p}$)

Algorithm 1: Pseudocode for greedy algorithm to optimize preamble sequence $\mathbf{p}$.

of merit F improves. For each subcarrier v this process is repeated until F cannot be improved anymore. After the phases of all $d \cdot K$ nonzero components have been optimized, the process starts over going through all nonzero DFT-components P_v again. This is repeated until F does not improve further. Then, the step size $\Delta\phi$ is divided by a factor c, and another round of phase optimizations is performed. After a certain number I of phase-increment updates (outer iterations) the algorithm is terminated. The resulting preamble $\mathbf{p}$ is accepted if F exceeds a certain threshold. Otherwise the greedy algorithm is run again with a different starting sequence. The pseudocode of this algorithm is shown in Algorithm 1.

3.3.3. Parameter adjustment

Once a preamble sequence has been generated, we need to determine the AGC reference value a_{ref} and the synchronization threshold t_{sync}.

A relatively small value of a_{ref} prevents clipping of the preamble while a larger value better suppresses impulse noise. As a good compromise between these conflicting constraints, we choose a_{ref} such that the maximum amplitude of the VGA output (after the soft limiter in Figure 2) is between 2 dB and 8 dB higher than the average amplitude of the preamble signal. The particular value depends on the application. For example, 2 dB is chosen for signal constellations of small size [e.g., quaternary phase-shift keying (QPSK)] and in an environment with frequent and strong impulse noise, while 8 dB is chosen for transmission with higher order modulation over medium voltage lines, which are less affected by impulse noise.

The proper choice of t_{sync} should maximize the probability of detection of the preamble while at the same time it should minimize the probability of a false alarm [31]. Successful synchronization is accomplished if after transmission of the preamble

$$M_{\text{sync}}[n] > t_{\text{sync}} \quad \text{for } 0 \leq n - (n_0 + N - 1) \leq n_\Delta, \qquad (21)$$

where n_Δ is the allowed detection window for synchronization for which demodulation of an OFDM packet is deemed possible (cf., e.g., [32, Table 1]). A false alarm occurs if no preamble was transmitted and $M_{\text{sync}}[n]$ exceeds t_{sync}. For a channel with additive white Gaussian noise (AWGN), that is, impulse noise is not present, closed-form expressions for the probability of successful synchronization P_s for $n_\Delta = 0$ and for the false alarm probability P_f are derived in the appendix. Evaluation of these expressions provides an initial value for t_{sync}, which is fine-tuned based on performance evaluations for a designed preamble as illustrated in the next section.

4. PERFORMANCE EVALUATION AND DISCUSSION

In this section, we present performance results for different preamble sequences. In particular, we choose one exemplary preamble generated by the greedy algorithm in Table 1 and compare it with two conventional preambles. The three preambles are described in Section 4.1, and the numerical results are presented in Section 4.2.

4.1. Preamble sequences

The exemplarily chosen preamble sequence has a total length of $K = 44$ samples with a synchronization part of $N = 35$ samples, which leaves $P = 9$ samples as the AGC-postfix. This preamble was designed with $d = 0.82$ in (14) (according to [24]), and it will be referred to as "designed preamble" and denoted by $\mathbf{p}_{\text{design}}$ in the following.

The two reference preambles are formed of, respectively, (a) a polyphase Barker sequence of length $N = 35$ and (b) a CAZAC sequence of length $N = 36$ as the synchronization part, and a linear Chirp sequence of length $P = 9$ as the

Table 1: Preamble sequences considered for performance evaluation.

$\mathbf{p}_{\text{design}}$	$-0.5186 - 0.8550j$, $0.6850 - 0.7266j$, $-0.1877 - 0.7345j$, $-0.7216 - 0.6922j$, $0.5752 - 0.1566j$, $0.5706 + 0.4945j$, $-0.1572 + 0.9843j$, $-0.7578 + 0.5299j$, $-0.2674 + 0.9012j$, $0.4711 + 0.8298j$, $0.1805 - 0.9835j$, $0.4024 - 0.4687j$, $-0.1827 + 0.9731j$, $-0.5384 - 0.2965j$, $-0.3448 - 0.5852j$, $-0.5189 + 0.5293j$, $0.6822 + 0.3166j$, $0.1691 + 0.7074j$, $-0.9553 + 0.2955j$, $0.5620 - 0.5343j$, $0.9510 + 0.2284j$, $0.2333 - 0.4250j$, $0.5995 - 0.4960j$, $0.1652 + 0.3264j$, $-0.4507 + 0.4647j$, $0.7754 + 0.6266j$, $0.5838 - 0.8082j$, $-0.6306 - 0.4283j$, $-0.0658 + 0.7983j$, $-0.7393 + 0.2733j$, $-0.9410 + 0.3381j$, $0.0238 - 0.8147j$, $-0.4497 - 0.5202j$, $-0.5574 + 0.4589j$, $-0.9053 - 0.4245j$, $-0.6832 + 0.5710j$, $-0.2192 + 0.6326j$, $-0.9379 + 0.3378j$, $0.0285 + 0.8345j$, $0.4634 - 0.5978j$, $-0.5754 - 0.5823j$, $-0.3050 + 0.5518j$, $-0.1199 + 0.6979j$, $-0.8711 + 0.0664j$
$\mathbf{p}_{\text{Barker}}$	$1, 1, -0.0567 + 0.9984j$, $0.4157 + 0.9095j$, $-0.9721 + 0.2345j$, $-0.6740 + 0.7388j$, $0.9619 - 0.2735j$, $0.1629 - 0.9867j$, $0.9247 - 0.3807j$, $0.5197 - 0.8544j$, $-0.9534 - 0.3018j$, $0.5569 + 0.8306j$, $0.8013 + 0.5983j$, $0.9871 + 0.1602j$, $0.8275 - 0.5615j$, $0.9010 - 0.4340j$, $0.9104 + 0.4137j$, $-0.9262 + 0.3771j$, $0.3604 - 0.9328j$, $0.5160 - 0.8566j$, $-0.8515 + 0.5244j$, $-0.3887 + 0.9214j$, $-0.7802 + 0.6255j$, $0.4477 - 0.8942j$, $-0.6259 + 0.7799j$, $-0.5798 + 0.8148j$, $0.9476 - 0.3194j$, $-0.6415 + 0.7671j$, $-0.4295 - 0.9031j$, $0.2783 + 0.9605j$, $0.7823 - 0.6230j$, $-0.9245 + 0.3812j$, $0.5104 - 0.8600j$, $-0.3007 + 0.9537j$, $-0.2693 - 0.9631j$, $0.3826 + 0.9238j$, $-0.5877 + 0.8089j$, $-0.9968 + 0.0785j$, $-0.8089 - 0.5877j$, $-0.3826 - 0.9238j$, $0 - 0.9999j$, $0.2334 - 0.9723j$, $0.3090 - 0.9510j$, $0.2334 - 0.9723j$
$\mathbf{p}_{\text{CAZAC}}$	$1, 1, 1, 1, 0.8660 + 0.5j$, $0.5 + 0.8660j$, $1, 0.5 + 0.8660j$, $-0.5 + 0.8660j$, $-1, -j$, $1, 1, -0.5 + 0.8660j$, $-0.5 - 0.8660j$, $1, -0.8660 + 0.5j$, $0.5 - 0.8660j$, $1, -1$, 1, -1, $0.8660 + 0.5j$, $-0.5 - 0.8660j$, $1, -0.5 - 0.8660j$, $-0.5 + 0.8660j$, $1, -j$, $-1, 1, 0.5 - 0.8660j$, $-0.5 - 0.8660j$, $-1, -0.8660 + 0.5j$, $-0.5 + 0.8660j$, $0.3826 + 0.9238j$, $-0.5877 + 0.8089j$, $-0.9968 + 0.0785j$, $-0.8089 - 0.5877j$, $-0.3826 - 0.9238j$, $-0.9999j$, $0.2334 - 0.9723j$, $0.3090 - 0.9510j$, $0.2334 - 0.9723j$

AGC-postfix, that is, the total lengths are (a) $K = 44$ and (b) $K = 45$ samples and thus (practically) the same as for the designed preamble. The Barker and CAZAC sequences are taken from [19, 33], respectively. These two preambles will be referred to as "Barker preamble" and "CAZAC preamble" and denoted by $\mathbf{p}_{\text{Barker}}$ and $\mathbf{p}_{\text{CAZAC}}$, respectively. We note that Barker, CAZAC, and also Chirp sequences are commonly used for synchronization purposes (cf., e.g., [1, 2, 5, 20]) and that they are well suited for AGC adjustment due to their constant envelope. For completeness the coefficients of the three considered preambles are printed in Table 1.

We would like to stress the point that, by design, the transmit signal (at the DAC output) corresponding to $\mathbf{p}_{\text{design}}$ satisfies the adopted spectral constraint, which is that about 9% at each side of the frequency band are used as guard band to achieve a signal suppression of larger than 20 dB with practical, low-delay filters. The spectra of the Barker and CAZAC preamble signals, on the other hand, are considerably wider and *exceed* the bandwidth B_s of the OFDM payload signal.

4.2. Numerical results

We now compare the three preambles with respect to their transmit-signal and correlation properties (Section 4.2.1), synchronization performance in AWGN and multipath channels and robustness against carrier frequency offsets and false synchronization to adjacent channel signals (Section 4.2.2), and suitability for fast AGC adjustment (Section 4.2.3).

4.2.1. Preamble signals

The complex envelopes of $\mathbf{p}_{\text{design}}$, $\mathbf{p}_{\text{Barker}}$, and $\mathbf{p}_{\text{CAZAC}}$ are plotted in Figure 5, where the maximal magnitude is normalized to one. While the Barker and CAZAC preambles have a constant envelope, the envelope of the designed preamble fluctuates. This is not surprising considering that we imposed the "hard" spectral constraint that only 82% of the subcarriers are active.

For the example of a carrier frequency of $f_c = 225$ kHz and an OFDM-signal bandwidth of $B_s = 140.5$ kHz, Figure 6 shows the DAC output signals for the different preambles (the plotted curves are 6-time oversampled signals). The maximal amplitude is again normalized to one. We observe that in the domain of the actually transmitted signals also the amplitudes of the Barker and CAZAC preambles vary significantly due to bandpass filtering. In fact, the PAPRs of these sequences are about 1.9 dB and 1.2 dB *higher* than that of the designed preamble, that is, for the same peak amplitude the transmit powers are *reduced* by a factor of $c_1 \approx 0.65$ and $c_2 \approx 0.76$, respectively. This is a clear advantage for the designed preamble and can be directly attributed to the incorporation of PAPR-related measures into the figure of merit F (20) used for preamble optimization.

The DAC output signals shown in Figure 6 are processed in the receiver (see Figure 1) with an appropriately adjusted and constant AGC gain (see Section 4.2.3 for a discussion

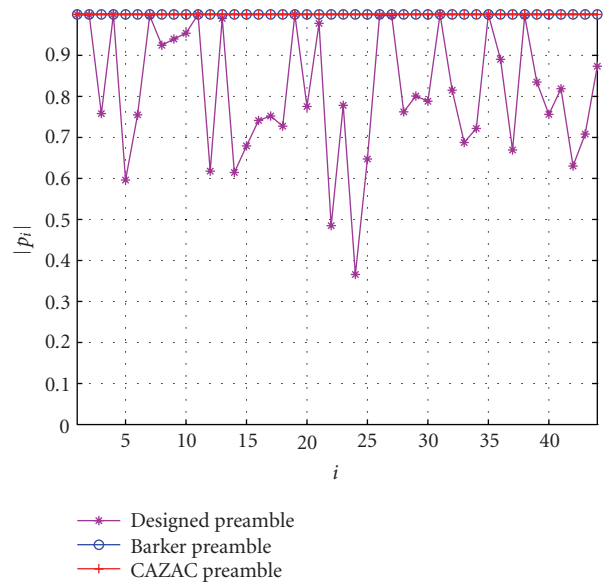

FIGURE 5: Magnitudes of the three preamble sequences considered for numerical evaluation and comparison.

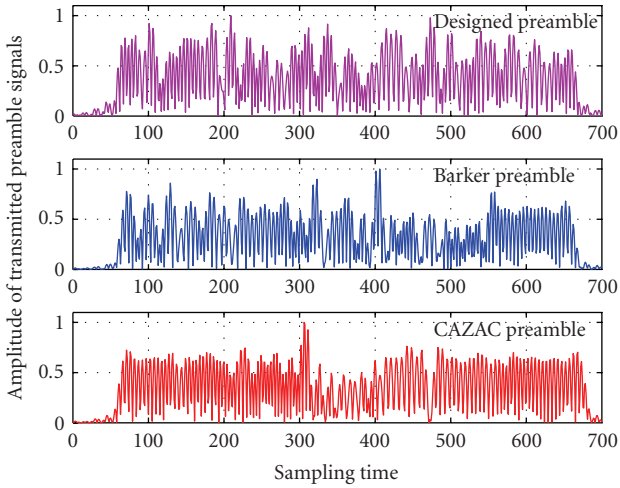

FIGURE 6: Magnitudes of the three preamble signals after the DAC (carrier frequency is $f_c = 225$ kHz and OFDM-signal bandwidth is $B_s = 140.5$ kHz, signals are 6-time oversampled).

on AGC adjustment) and passed to the synchronization unit (see Figure 3). The measured correlator outputs $M[n]$ (6) are shown in Figure 7. It is interesting to observe that the correlation peak of the designed preamble is considerably larger than those of the Barker and CAZAC preambles. This is mainly due to the higher transmit power of the designed preamble for constant maximal amplitude as explained above. The designed preamble also achieves a high peak-to-side-peak ratio at the correlator output, which is comparable to those for the Barker and CAZAC preambles.

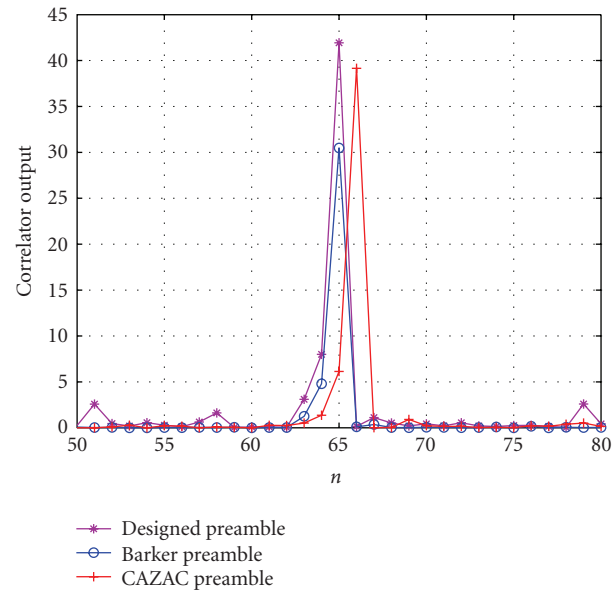

FIGURE 7: Correlator output $M[n]$ [see (6)] for noise-free transmission of preamble signals.

4.2.2. *Synchronization performance*

To evaluate the synchronization performance, we first consider the idealized scenario of an AWGN channel and that the preamble signals are not distorted by filtering or clipping, that is, the sequences $\mathbf{p}_{\text{design}}$, $\sqrt{c_1} \cdot \mathbf{p}_{\text{Barker}}$, and $\sqrt{c_2} \cdot \mathbf{p}_{\text{CAZAC}}$ plus AWGN are received at the synchronization unit, with c_1 and c_2 as given above to account for the lower transmit power for the Barker and CAZAC preamble, respectively. Under these assumptions we evaluate the expressions derived in the appendix for the probability of successful synchronization P_s and the false alarm probability P_f. Figure 8 shows the numerical results in terms of the threshold t_{sync} for which, respectively, $P_s = 1 - 10^{-5}$ and $P_f = 10^{-5}$ are achieved as function of the SNR $10\log_{10}(P_t/\sigma_w^2)$, where P_t is the transmit power for the designed preamble. Synchronization metrics $M_{\text{sync}}[n]$ with $L = 2, 4, 8$ are considered. It can be seen that for SNRs larger than about 4 dB for $L = 2$ and 8 dB for $L = 8$ thresholds can be found such that $P_s > 1 - 10^{-5}$ and $P_f < 10^{-5}$. The particular value of t_{sync} should be chosen as function of L, for example, $t_{\text{sync}} = 15$ is suitable for $L = 2$, while $t_{\text{sync}} \gtrsim 20$ is appropriate for $L = 8$. The designed sequence performs best in that the SNR value, at which the curves for successful synchronization and false alarm intersect, is the smallest. It can be expected that this improvement becomes more pronounced when the effects of filtering are taken into account, since the values for t_{sync} required for $P_f = 10^{-5}$ will increase for the Barker and CAZAC preambles if the actual, nonconstant signal envelope is taken into account.

Next, we consider synchronization in a multipath environment. As an illustrative example particularly relevant for transmission in SFNs, we assume a channel impulse response with two taps of equal amplitude and spaced by ΔT.

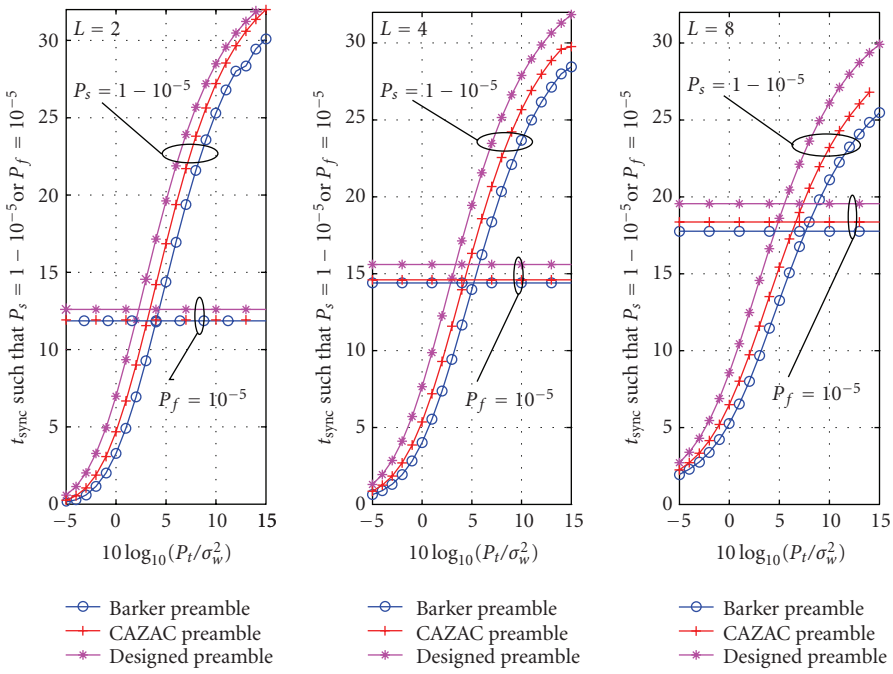

FIGURE 8: Threshold t_{sync} as function of SNR $10\log_{10}(P_t/\sigma_w^2)$. t_{sync} is adjusted such that $P_s = \Pr\{M_{\text{sync}}[n_0 + N - 1] > t_{\text{sync}}\} = 1 - 10^{-5}$ if preamble was sent and $P_f = \Pr\{M_{\text{sync}}[n] > t_{\text{sync}}\} = 10^{-5}$ if no preamble was sent, respectively. Analytical results (see the appendix).

The phases of the two taps are rotated to each other by 0, $\pi/2$, π, and $3\pi/2$ as sample values for possible phase differences. The preambles are transmitted through such a channel and processed at the receiver assuming an appropriately adjusted AGC with constant gain. In the synchronization unit, the metric $M_{\text{sync}}[n]$ with $L = 2, \ldots, 8$ is evaluated, and the allowed detection window for synchronization is chosen as $n_\Delta = L - 1$. Figure 9 shows the maximal values $\widehat{M}_{\text{in}}$ and $\widehat{M}_{\text{out}}$ of $M_{\text{sync}}[n]$ for n falling *in*side this window, that is, $n_0 + N - 1 \le n < n_0 + N + n_\Delta$ and for n *out*side[2] this window, that is, $n < n_0 + N - 1$, respectively, as function of $\Delta T f_s$ for all three preambles. For clarity, noise-free transmission is assumed. We observe that the full channel energy (equally distributed over the two taps) can be captured with increasing L, that is, $\widehat{M}_{\text{in}}$ reaches large values also for $0 \le \Delta T f_s \le L$, which confirms the suitability of the devised synchronization metric $M_{\text{sync}}[n]$ for multipath channels. We further observe that $\widehat{M}_{\text{in}}$ is always larger than $\widehat{M}_{\text{out}}$, which is a necessary requirement for successful synchronization since noise-free transmission is assumed. However, the margin between $\widehat{M}_{\text{in}}$ and $\widehat{M}_{\text{out}}$ is noticeably improved for the designed preamble when compared to the Barker and CAZAC preambles. Hence, we conclude that the designed preamble is advantageous for synchronization in a multipath environment. Again, we can attribute this improvement to the preamble design as devised in Section 3.3, which explicitly considers synchronization in multipath channels and correlation with $L > 1$.

To assess the robustness of synchronization against carrier frequency offset, Figure 10 shows the threshold t_{sync} for which $P_s = 1 - 10^{-5}$ is achieved as a function of the normalized offset $\Delta f_c/f_s$ and for synchronization with $L = 2, 4, 8$. The numerical results are obtained from the expressions presented in the appendix and the same set up as in Figure 8 is applied, and the SNR is chosen as $10\log_{10}(P_t/\sigma_w^2) = 10$ dB. For clarity, only the designed preamble and the Barker preamble are considered. We observe that, for both preambles, the degradation of the synchronization threshold is fairly moderate for $|\Delta f_c/f_s| < 0.002$ and becomes more significant with increasing frequency offset, especially for smaller values of L. Since $|\Delta f_c/f_s| = 0.002$ corresponds to a maximal absolute offset of about ± 30 Hz considering the smallest sampling rate of about $f_s = 15$ kHz, and since the highest possible carrier frequency is about $f_c = 0.5$ MHz, a local oscillator offset of 60 ppm would be acceptable. This is a much less stringent requirement on the local oscillator stability than those imposed by the OFDM transmission system. Thus, we conclude that the potential carrier frequency offsets are well coped with by the devised synchronization method.

Finally, the robustness against false synchronization in the presence of adjacent channel signals is considered. It should be noted that for the large dynamic of, say, 120 dB of AGC and ADC required in PLC systems, the typical attenuation of about, say, 60 dB of adjacent channel signals is not sufficient to prevent false synchronization. As exemplary system parameters, we choose a transmitter carrier frequency

[2] It should be noted that the synchronization will always lock on to the first n for which $M_{\text{sync}}[n] > t_{\text{sync}}$. Therefore, we do not consider maxima of $M_{\text{sync}}[n]$ for $n \ge n_0 + N + n_\Delta$.

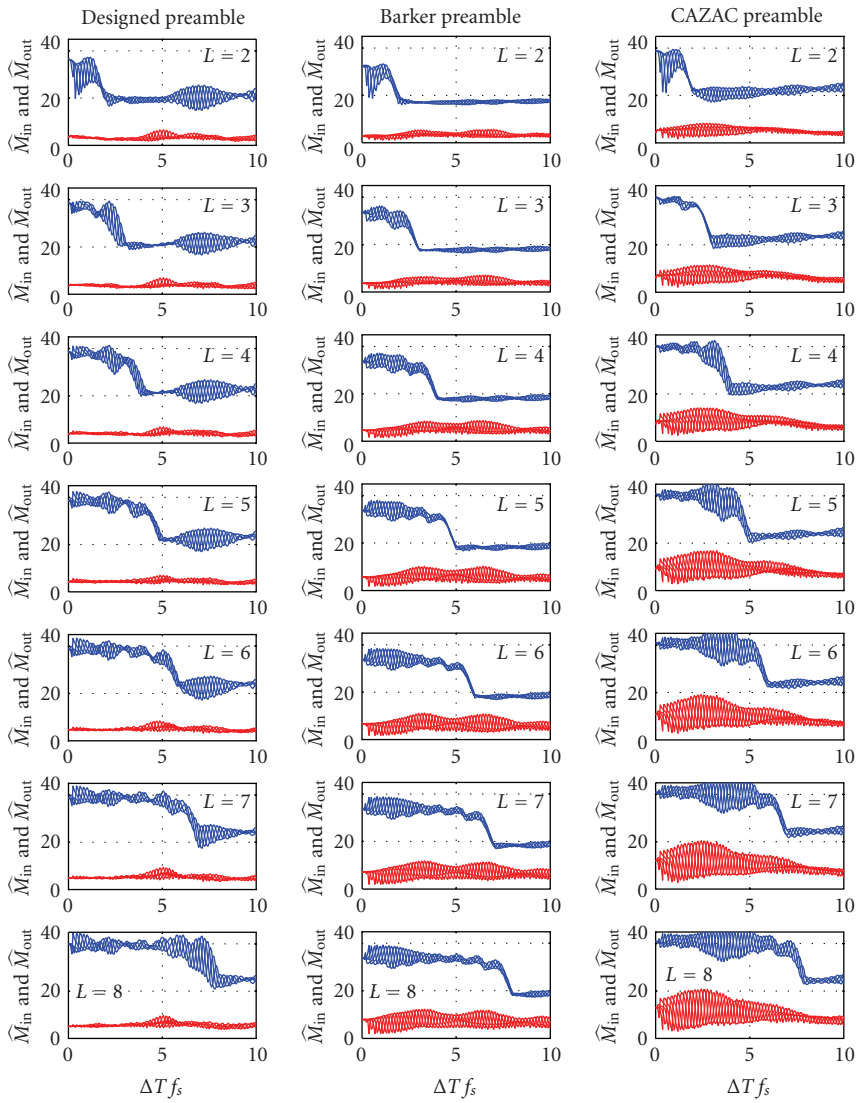

FIGURE 9: $M_{\text{sync}}[n]$ as function of $\Delta T f_s$ for a noise-free multipath channel with two paths spaced by ΔT and with phase offsets of $[0, \pi/2, \pi, 3\pi/2]$. Top four curves in each graph: $n_0 + N - 1 \leq n < n_0 + N + L - 1$. Bottom four curves in each graph: $n < n_0 + N - 1$. From top to bottom: $L = 2, \ldots, 8$. From left to right: designed preamble, Barker preamble, and CAZAC preamble. Simulation results.

of $f_c = 230\,\text{kHz}$ and an OFDM-system bandwidth of $B_s = 60.4\,\text{kHz}$. The receiver carrier frequency is $f_c + \Delta f_c$ with a variable offset of $-230\,\text{kHz} < \Delta f_c < 270\,\text{kHz}$ to cover the entire frequency band. The AGC gain is held constant and $L = 8$ is considered, since we found the strongest effects of false synchronization for larger correlation windows. In Figure 11, we show the value of $M_{\text{sync}}[n]$ for the actual synchronization time $n_0 + N - 1 \leq n < n_0 + N + L - 1$ (solid lines) and for $n < n_0 + N - 1$ (dashed lines), that is, too early synchronization, for all three preambles. Of course, synchronization to an adjacent channel signal is always unwanted, regardless of whether the synchronization locks on to the correct point in time or not. We observe that the designed preamble is considerably more robust against false synchronization. For both Barker and CAZAC preamble large metrics $M_{\text{sync}}[n]$ occur for $|\Delta f_c| > 0$. In case of the CAZAC preamble the ambiguities are a result of its linear Chirp-like structure (cf. [34] and the design tool [33]). The designed sequence shows the best performance because of the randomly chosen initial phases of its DFT coefficients, which renders a systematic dependency between these coefficients unlikely.

4.2.3. AGC adjustment

Due to its dynamic gain at the beginning of a received preamble signal, the AGC influences the synchronization performance. We found in various simulations of synchronization with active AGC that the effect of the nonlinearities on the correlation gain is quite similar for the different preambles and not severe in case of an appropriately adjusted AGC

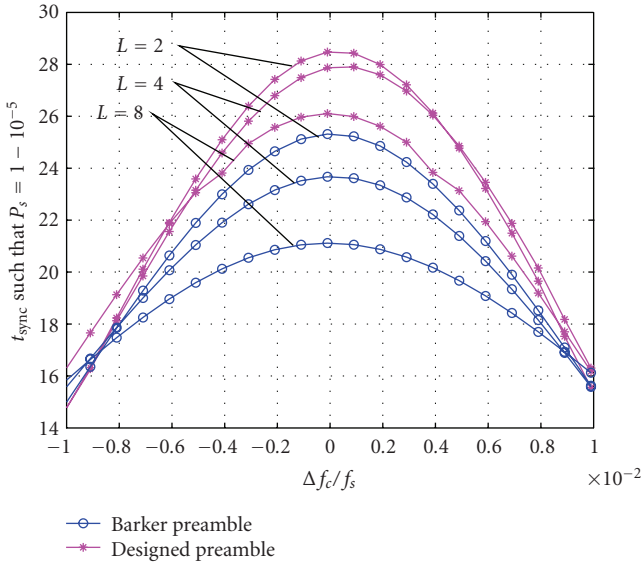

FIGURE 10: Threshold t_{sync} as function of normalized frequency offset $\Delta f/f_s$ for $10\log_{10}(P_t/\sigma_w^2) = 10$ dB. t_{sync} is adjusted such that $P_s = \Pr\{M_{\text{sync}}[n_0 + N - 1] > t_{\text{sync}}\} = 1 - 10^{-5}$ if preamble was sent for $L = 2, 4, 8$. Analytical results.

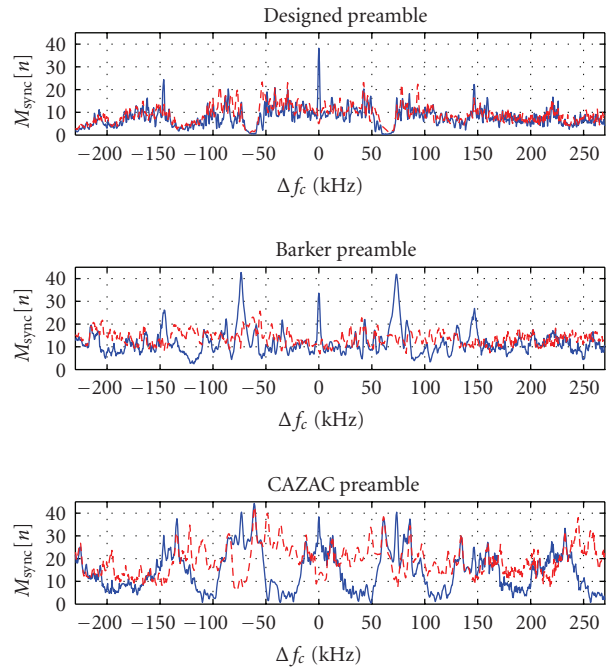

FIGURE 11: $M_{\text{sync}}[n]$ for $n_0 + N - 1 \le n < n_0 + N + L - 1$ (solid lines) and for $n < N + n_0 - 1$ (dashed lines) when preamble signal was sent with a frequency offset Δf_c. Carrier frequency $f_c = 230$ kHz, OFDM-signal bandwidth $B_s = 60.4$ kHz, noise-free channel, and synchronization with $L = 8$. Simulation results.

speed. We therefore concentrate on the suitability of the preamble signals for AGC adjustment. A preamble is deemed suitable if the AGC gain converges fast to a final value with little fluctuation before reaching this value in order to allow for sufficient averaging (I-circuit) of noise effects.

Figures 12 and 13 illustrate the adjustment of the AGC gain for a relatively narrow OFDM-signal bandwidth of $B_s = 15.1$ kHz (Figure 12) and a relatively high bandwidth of $B_s = 352$ kHz (Figure 13). The step size of gain of the VGA is 2 dB and the moving-average parameter [see (1)] is $N_{\text{AGC}} = 64$ for the narrowband signal and $N_{\text{AGC}} = 32$ for the wideband signal. The maximal ADC output corresponds to a unit amplitude, and $a_{\text{ref}} = 0.4$ is adjusted (see Figure 2), which, for example, corresponds to an about 5 dB margin between maximal and effective value of a sine signal. The preambles are received without noise and preceded by an all-zero sequence of 70 samples. Taking filter delay time into account a constant AGC gain should be reached after between 111 and 119 received samples. It can be seen that, for both signal bandwidths, the designed preamble leads to a considerably faster and more stable gain adjustment than the Barker and CAZAC preambles. Especially the Barker preamble causes large variations of up to 8 dB of the AGC gain in the critical range between 111 to 119 samples. This is not acceptable considering that the difference between maximal and average amplitude after the soft limiter (see Figure 2) should be not more than 8 dB in order to suppress impulse noise. We conclude that the devised optimization of the preamble, taking requirements for AGC adjustment into account, has resulted in an improved performance also in this respect.

5. CONCLUSIONS

In this paper, we have presented a comprehensive approach for the design of preamble sequences for fast burst synchronization in PLC systems. We have concentrated on systems operating below 500 kHz with data rates not exceeding 500 kbps (which are typical for various network applications), for which carrier and sampling frequency synchronization are not necessary. The proposed optimization method takes important practical requirements, in particular the need for spectral shaping and for fast AGC adjustment, into account. The most prominent properties of the power line channel, which are multipath propagation, highly varying path loss, and disturbance by impulse noise, are explicitly accounted for through the devised AGC structure and the novel synchronization metric. We have also devised a suboptimal stochastic optimization algorithm to efficiently search for preamble sequences which maximize the developed figure of merit. An extensive performance comparison of a newly designed and two conventional preamble sequences has shown that the designed sequence yields the best results both in terms of synchronization in various transmission environments and in terms of AGC adjustment. Thus we believe that the presented framework is particularly useful for system engineers looking for an in-(m)any-respect(s) good solution.

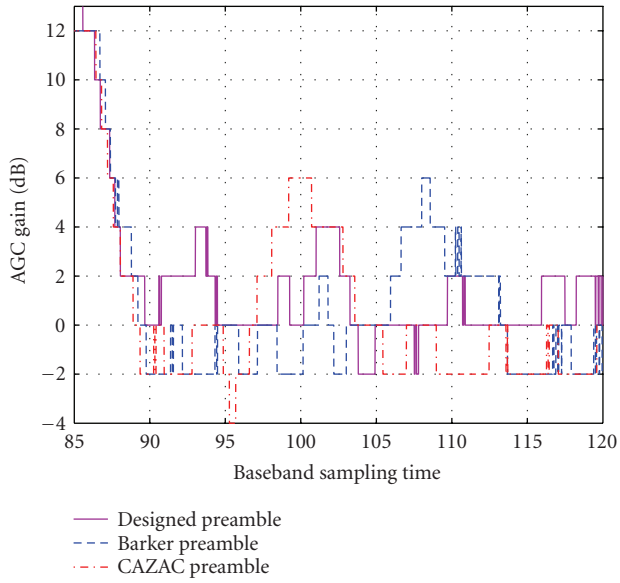

FIGURE 12: Adjustment of AGC gain while preamble is received (noise-free transmission). OFDM-signal bandwidth is $B_s = 15.1$ kHz and carrier frequency is $f_c = 40$ kHz.

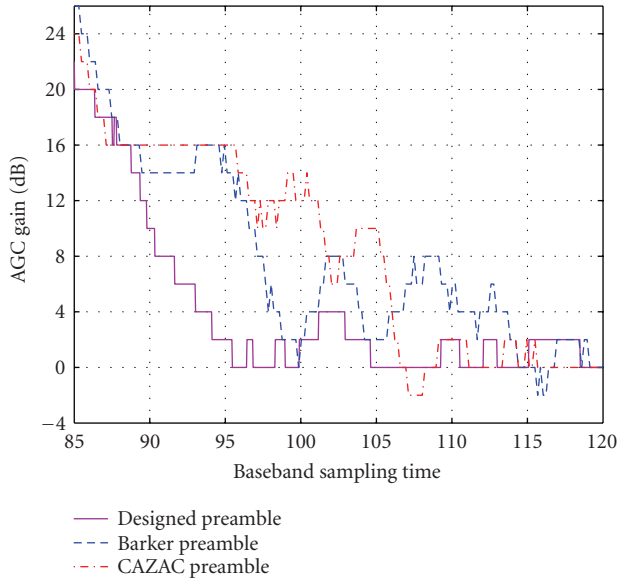

FIGURE 13: Adjustment of AGC gain while preamble is received (noise-free transmission). OFDM-signal bandwidth is $B_s = 352$ kHz and carrier frequency is $f_c = 335$ kHz.

APPENDIX

In this appendix, we derive (semi-)analytical expressions for the probabilities of false alarm and successful detection. For simplicity, a transmission delay of $n_0 = 0$ is assumed in the following.

A.1. False alarm probability P_f

A synchronization event at any time n is declared a false alarm if no preamble was sent. Hence, it follows from (10) that

$$P_f \triangleq \Pr\{M_{\text{sync}}[n] > t_{\text{sync}}\} \tag{A.1}$$

$$= \Pr\left\{\sum_{l=0}^{L-1}\left|\sum_{i=0}^{N-1} w[n-l-i]s_{N-i}^{*}\right|^2 > t_{\text{sync}}^2 \sum_{i=0}^{N+L-2}|w[n-i]|^2\right\}, \tag{A.2}$$

where $w[n]$ denotes complex AWGN with variance σ_w^2. After straightforward manipulations, we can rewrite P_f in (A.2) as the quadratic form

$$P_f = \Pr\{\mathbf{w}^H\mathbf{F}\mathbf{w} < 0\}, \tag{A.3}$$

where we used the definitions

$$\mathbf{F} \triangleq t_{\text{sync}}^2\mathbf{I}_{N+L-1} - \sum_{l=0}^{L-1}\bar{\mathbf{s}}_l\bar{\mathbf{s}}_l^H,$$

$$\mathbf{w} \triangleq [w[n]\, w[n-1]\, \cdots w[n-L-N+2]]^T, \tag{A.4}$$

$$\bar{\mathbf{s}}_l \triangleq [\underbrace{0\cdots 0}_{l}\, s_N\, s_{N-1}\, \cdots\, s_1\, \underbrace{0\cdots 0}_{L-1-l}]^T.$$

We note that $\mathbf{F}$ has $N-1$ positive eigenvalues t_{sync} and additional L eigenvalues, which are possibly negative. Assuming that all negative eigenvalues are distinct, and since $\mathbf{w}$ is a vector of independent zero-mean Gaussian random variables, the false alarm probability in (A.3) can be expressed as

$$P_f = \sum_{\lambda_i<0}\prod_{\substack{l=0\\ l\neq i}}^{N+L-2}\frac{1}{1-\lambda_l/\lambda_i}, \tag{A.5}$$

where λ_i, $0 \le i \le N+L-2$, are the eigenvalues of $\mathbf{F}$ [35, Appendix A]. If some negative eigenvalues have multiplicity larger than one, a somewhat more complicated expression results (cf., e.g., [36, Section III.A]). We note that due to the normalization used for $M_{\text{sync}}[n]$ in (10), P_f is independent of the noise power σ_w^2.

A.2. Probability of successful detection P_s

A synchronization event is declared successful, if a preamble was transmitted and

$$M_{\text{sync}}[n] > t_{\text{sync}} \tag{A.6}$$

for an n within the synchronization window $[N-1, N-1+n_\Delta]$. In the following, we assume $n_\Delta = 0$, which simplifies the derivation as we do not need to consider the union of events $M_{\text{sync}}[n] > t_{\text{sync}}$ for multiple n. Following similar steps as in (A.1)–(A.3), we arrive at

$$P_s = \Pr\{\mathbf{y}^H\mathbf{F}\mathbf{y} < 0\}, \tag{A.7}$$

where

$$y[n] = f(p,n) + w[n],$$
$$\mathbf{y} \triangleq [y[n]\, y[n-1] \cdots y[n-L-N+2]]^T, \tag{A.8}$$

and $f(\mathbf{p},n)$ is assumed to be a linear function of the preamble $\mathbf{p}$, which depends on the transmission channel. For example, $f(\mathbf{p},n) = p_{n+1}$, $0 \le n < K$ and zero otherwise, for an AWGN channel. It is also straightforward to take multipath transmission and a carrier frequency offset into account. We observe that $\mathbf{y}$ is a vector of independent Gaussian random variables with mean

$$\overline{\mathbf{y}} \triangleq [f(\mathbf{p},n)\, f(\mathbf{p},n-1) \cdots f(\mathbf{p},n-L-N+2)]^T \tag{A.9}$$

and autocorrelation matrix $\sigma_w^2 \mathbf{I}_{N+L-1}$.

Following the exposition in [37, Appendix B], we can express P_s as

$$P_s = \frac{1}{2\pi j} \int_{\alpha - j\infty}^{\alpha + j\infty} \frac{\Phi(s)}{s} ds, \tag{A.10}$$

where

$$\Phi(s) = \frac{\exp\left(-s\overline{\mathbf{y}}^H \left(\mathbf{F}^{-1} + s\mathbf{I}_{N+L-1}\sigma_w^2\right)^{-1}\overline{\mathbf{y}}\right)}{\det\left(\mathbf{I}_{N+L-1} + s\sigma_w^2\mathbf{F}\right)} \tag{A.11}$$

and $\alpha > 0$ lies in the region of convergence of $\Phi(s)$. Due to the essential singularities of $\Phi(s)$ originating from the exponential term, we choose to numerically evaluate (A.10) using a Gauss-Chebyshev quadrature rule with q nodes [38]

$$P_s = \frac{1}{q} \sum_{i=1}^{q/2} \left[\Re\{\Phi(\alpha + j\alpha\tau_i)\} + \tau_i \Im\{\Phi(\alpha + j\alpha\tau_i)\}\right] + E_q, \tag{A.12}$$

where $\tau_i = \tan[(2i-1)\pi/(2q)]$ and the error term E_q becomes negligible for reasonably large q (of the order of a few hundreds).

ACKNOWLEDGMENTS

The work in this paper was presented in part at the 2007 IEEE International Symposium on Power Line Communications and Its Applications (ISPLC), Pisa, Italy, March 26–28, 2007. The work of Lutz Lampe was supported in part by the National Sciences and Engineering Research Council (NSERC) of Canada.

REFERENCES

[1] J. Massey, "Optimum frame synchronization," *IEEE Transactions on Communications*, vol. 20, no. 2, pp. 115–119, 1972.

[2] R. Scholtz, "Frame synchronization techniques," *IEEE Transactions on Communications*, vol. 28, no. 8, part 2, pp. 1204–1213, 1980.

[3] S. A. Fechtel and H. Meyr, "Fast frame synchronization, frequency offset estimation and channel acquisition for spontaneous transmission over unknown frequency-selective radio channels," in *Proceedings of IEEE International Symposium on Personal, Indoor and Mobile Radio Communications (PIMRC '93)*, pp. 229–233, Yokohama, Japan, September 1993.

[4] IEEE 802.11a, "Wireless LAN Medium Access Control (MAC) and Physical Layer (PHY) Specifications: High-Speed Physical Layer in the 5 GHz Band," 1999.

[5] IEEE 802.15.3, "Wireless Medium Access Control (MAC) and Physical Layer (PHY) Specifications for High Rate Wireless PANs," 2003.

[6] M. K. Lee, R. E. Newman, H. A. Latchman, S. Katar, and L. Yonge, "HomePlug 1.0 powerline communication LANs—protocol description and performance results," *International Journal of Communication Systems*, vol. 16, no. 5, pp. 447–473, 2003.

[7] S. Müller-Weinfurtner, *OFDM for Wireless Communications: Nyquist Windowing, Peak-Power Reduction, and Synchronization*, Shaker, Aachen, Germany, 2000.

[8] N. Pavlidou, A. J. Han Vinck, J. Yazdani, and B. Honary, "Power line communications: state of the art and future trends," *IEEE Communications Magazine*, vol. 41, no. 4, pp. 34–40, 2003.

[9] G. Bumiller, T. Sauter, G. Pratl, and A. Treytl, "Secure and reliable wide-area power-line communication for soft-real-time applications within REMPLI," in *Proceedings of the 9th International Symposium on Power Line Communications and Its Applications (ISPLC '05)*, pp. 57–60, Vancouver, British Columbia, Canada, April 2005.

[10] M. H. Shwehdi and A. Z. Khan, "A power line data communication interface using spread spectrum technology in home automation," *IEEE Transactions on Power Delivery*, vol. 11, no. 3, pp. 1232–1237, 1996.

[11] P. van Rensburg and H. Ferreira, "Automotive power-line communications: favourable topology for future automotive electronic trends," in *Proceedings of the 7th International Symposium on Power-Line Communications and Its Applications (ISPLC '03)*, pp. 103–108, Kyoto, Japan, March 2003.

[12] M. Zimmermann and K. Dostert, "A multipath model for the powerline channel," *IEEE Transactions on Communications*, vol. 50, no. 4, pp. 553–559, 2002.

[13] M. Eriksson, "Dynamic single frequency networks," *IEEE Journal on Selected Areas in Communications*, vol. 19, no. 10, pp. 1905–1914, 2001.

[14] G. Bumiller, "Single frequency network technology for medium access and network management," in *Proceedings of the 6th International Symposium on Power-Line Communications and Its Applications (ISPLC '02)*, Athens, Greece, March 2002.

[15] F. J. C. Corripio, J. A. C. Arrabal, L. D. Del Río, and J. T. E. Muñoz, "Analysis of the cyclic short-term variation of indoor power line channels," *IEEE Journal on Selected Areas in Communications*, vol. 24, no. 7, pp. 1327–1338, 2006.

[16] S. Barmada, A. Musolino, and M. Raugi, "Innovative model for time-varying power line communication channel response evaluation," *IEEE Journal on Selected Areas in Communications*, vol. 24, no. 7, pp. 1317–1325, 2006.

[17] M. Zimmermann and K. Dostert, "Analysis and modeling of impulsive noise in broad-band powerline communications," *IEEE Transactions on Electromagnetic Compatibility*, vol. 44, no. 1, pp. 249–258, 2002.

[18] S. Golomb and R. Scholtz, "Generalized Barker sequences," *IEEE Transactions on Information Theory*, vol. 11, no. 4, pp. 533–537, 1965.

[19] M. Friese, "Polyphase Barker sequences up to length 36," *IEEE Transactions on Information Theory*, vol. 42, no. 4, pp. 1248–1250, 1996.

[20] A. Milewski, "Periodic sequences with optimal properties for channel estimation and fast start-up equalization," *IBM Journal of Research and Development*, vol. 27, no. 5, pp. 426–431, 1983.

[21] European Committee for Electrotechnical Standardization (CENELEC), "EN 50065-1: Signaling on Low-Voltage Electrical Installations in the Frequency Range 3 kHz-148.5 kHz," 2001.

[22] Association of Radio Industries and Businesses (ARIB), "STD-T84: Power Line Communication Equipment (10 kHz-450 kHz)", 2002.

[23] Federal Communication Commission (FCC), "ET Docket 04-37, FCC 04-245," October 2004.

[24] G. Bumiller and M. Deinzer, "Narrow band power-line chipset for telecommunication and Internet application," in *Proceedings of the 5th International Symposium on Power-Line Communications and Its Applications (ISPLC '01)*, pp. 353–358, Malmö, Sweden, April 2001.

[25] J. M. Khoury, "On the design of constant settling time AGC circuits," *IEEE Transactions on Circuits and Systems II: Analog and Digital Signal Processing*, vol. 45, no. 3, pp. 283–294, 1998.

[26] M. Antweiler and L. Bömer, "Merit factor of Chu and Frank sequences," *Electronics Letters*, vol. 26, no. 25, pp. 2068–2070, 1990.

[27] W.-G. Jeon, Y.-H. You, J.-T. Kim, et al., "Timing synchronization for IEEE 802.15.3 WPAN applications," *IEEE Communications Letters*, vol. 9, no. 3, pp. 255–257, 2005.

[28] S. E. Kocabaş and A. Atalar, "Binary sequences with low aperiodic autocorrelation for synchronization purposes," *IEEE Communications Letters*, vol. 7, no. 1, pp. 36–38, 2003.

[29] W. D. Warner and C. Leung, "OFDM/FM frame synchronization for mobile radio data communication," *IEEE Transactions on Vehicular Technology*, vol. 42, no. 3, pp. 302–313, 1993.

[30] O. Üreten, S. Tascioglu, N. Serinken, and M. Yilmaz, "Search for OFDM synchronization waveforms with good aperiodic autocorrelations," in *Proceedings of IEEE Canadian Conference on Electrical and Computer Engineering (CCECE '04)*, vol. 1, pp. 13–18, Niagara Falls, Canada, May 2004.

[31] H. L. van Trees, *Detection, Estimation, and Modulation Theory—Part I*, John Wiley & Sons, New York, NY, USA, 2001.

[32] G. Bumiller, "Verification of single frequency network transmission with laboratory measurements," in *Proceedings of IEEE International Symposium on Power Line Communications and Its Applications (ISPLC '06)*, pp. 27–32, Orlando, Fla, USA, March 2006.

[33] J. J. Benedetto and J. F. Ryan, "Software Package for CAZAC Code Generators and Doppler Shift Analysis," 2004, http://www.math.umd.edu/jjb/cazac.

[34] B. M. Popovic, "Generalized chirp-like polyphase sequences with optimum correlation properties," *IEEE Transactions on Information Theory*, vol. 38, no. 4, pp. 1406–1409, 1992.

[35] M. Barrett, "Error probability for optimal and suboptimal quadratic receivers in rapid Rayleigh fading channels," *IEEE Journal on Selected Areas in Communications*, vol. 5, no. 2, pp. 302–304, 1987.

[36] M. Brehler and M. K. Varanasi, "Asymptotic error probability analysis of quadratic receivers in Rayleigh-fading channels with applications to a unified analysis of coherent and noncoherent space-time receivers," *IEEE Transactions on Information Theory*, vol. 47, no. 6, pp. 2383–2399, 2001.

[37] M. Schwartz, W. Bennett, and S. Stein, *Communication Systems and Techniques*, McGraw-Hill, New York, NY, USA, 1966.

[38] E. Biglieri, G. Caire, G. Taricco, and J. Ventura-Traveset, "Computing error probabilities over fading channels: a unified approach," *European Transactions on Telecommunications*, vol. 9, no. 1, pp. 15–25, 1998.

Gerd Bumiller received the Diplom Univ. degree in electrical engineering from the University of Erlangen-Nürnberg, Germany, in 1997, with a thesis on improved receiver designs for DECT (digital enhanced cordless telecommunication) systems. He joined iAd GmbH, Germany, in 1997, where he was promoted leader of the communications system development group in 1998. Since 2000, he has been Director of technology development and responsible for all power line communications projects of iAd.

Lutz Lampe received the Diplom Univ. and the Ph.D. degrees in electrical engineering from the University of Erlangen-Nürnberg, Germany, in 1998 and 2002, respectively. He is currently an Assistant Professor at the Department of Electrical and Computer Engineering, the University of British Columbia. His main research interests lie in the areas of communications and information theory applied to wireless and power line transmission. He is corecipient of the Eurasip Signal Processing Journal Best Paper Award 2005, the Best Paper Award at the IEEE International Conference on Ultra-Wideband (ICUWB) 2006, and the Best Student Paper Awards at the European Wireless Conference 2000 and at the International Zurich Seminar 2002. In 2003, he received the Dissertation Award of the German Society of Information Techniques (ITG). He is an Editor for the IEEE Transactions on Wireless Communications and Associate Editor for the IEEE Transactions on Vehicular Technology, and serves as Vice-Chair of the IEEE Communications Society Technical Committee on Power Line Communications. He was General Chair of the 2005 International Symposium on Power Line Communications and Its Applications (ISPLC 2005) and Cochair of the General Symposium of the 2006 IEEE Global Telecommunications Conference (Globecom 2006).